Advanced Characterisation of a Coffee Fermenting Tank by Multi-distributed Wireless Sensors: Spatial Interpolation and Phase Space Graphs

E. C. Correa, T. Jiménez-Ariza, V. Díaz-Barcos, P. Barreiro, B. Diezma, R. Oteros, C. Echeverri, F. J. Arranz & M. Ruiz-Altisent

Food and Bioprocess Technology
An International Journal

ISSN 1935-5130

Food Bioprocess Technol
DOI 10.1007/s11947-014-1328-4

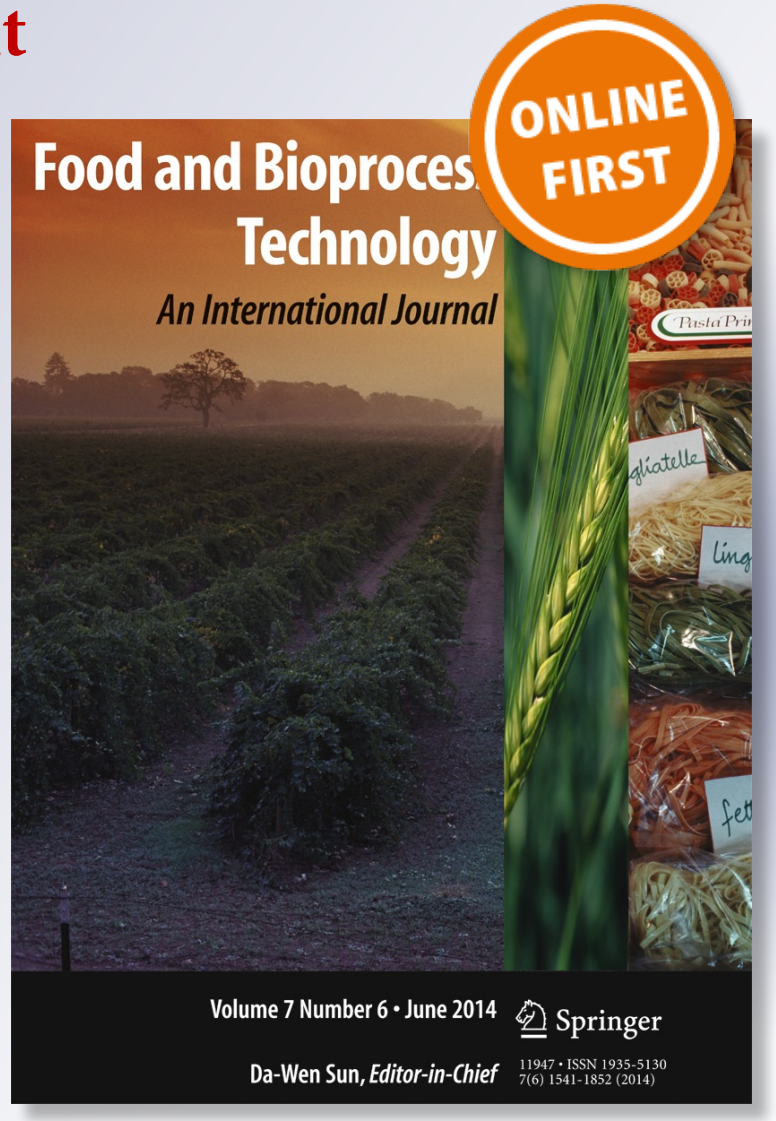

Springer

Food Bioprocess Technol
DOI 10.1007/s11947-014-1328-4

ORIGINAL PAPER

Advanced Characterisation of a Coffee Fermenting Tank by Multi-distributed Wireless Sensors: Spatial Interpolation and Phase Space Graphs

E. C. Correa · T. Jiménez-Ariza · V. Díaz-Barcos · P. Barreiro · B. Diezma · R. Oteros · C. Echeverri · F. J. Arranz · M. Ruiz-Altisent

Received: 31 January 2014 / Accepted: 30 April 2014

Abstract The fermentation stage is considered to be one of the critical steps in coffee processing due to its impact on the final quality of the product. The objective of this work is to characterise the temperature gradients in a fermentation tank by multi-distributed, low-cost and autonomous wireless sensors (23 semi-passive TurboTag® radio-frequency identifier (RFID) temperature loggers). Spatial interpolation in polar coordinates and an innovative methodology based on phase space diagrams are used. A real coffee fermentation process was supervised in the Cauca region (Colombia) with sensors submerged directly in the fermenting mass, leading to a 4.6 °C temperature range within the fermentation process. Spatial interpolation shows a maximum instant radial temperature gradient of 0.1 °C/cm from the centre to the perimeter of the tank and a vertical temperature gradient of 0.25 °C/cm for sensors with equal polar coordinates. The combination of spatial interpolation and phase space graphs consistently enables the identification of five local behaviours during fermentation (hot and cold spots).

Keywords Temperature · WSN · Attractor · Control · Food quality · Dynamic behaviour

E. C. Correa (✉) · T. Jiménez-Ariza · P. Barreiro · B. Diezma · M. Ruiz-Altisent
Laboratorio de Propiedades Físicas y Tecnologías Avanzadas en Agroalimentación; Departamento de Ingeniería Rural, E.T.S.I. Agrónomos, Universidad Politécnica de Madrid-CEI Moncloa, Av. Complutense s/n, Ciudad Universitaria, 28040 Madrid, Spain
e-mail: evacristina.correa@upm.es

T. Jiménez-Ariza
e-mail: tatiana.jimenez.ariza@upm.es

P. Barreiro
e-mail: pilar.barreiro@upm.es

B. Diezma
e-mail: belen.diezma@upm.es

M. Ruiz-Altisent
e-mail: margarita.ruiz.altisent@upm.es

E. C. Correa · V. Díaz-Barcos
Departamento de Ciencia y Tecnologías Aplicadas a la Ingeniería Técnica Agrícola; E.U.I.T. Agrícola, Universidad Politécnica de Madrid-CEI Moncloa, Av. Complutense s/n, Ciudad Universitaria, 28040 Madrid, Spain

R. Oteros · C. Echeverri
Supracafé, S.A. Torres Quevedo, 15-17. Polígono Industrial Prado de Regordoño, 28936 Móstoles, Madrid, Spain

F. J. Arranz
Grupo de Sistemas Complejos, ETSI Agrónomos, Universidad Politécnica de Madrid-CEI Moncloa, Av. Complutense s/n, Ciudad Universitaria, 28040 Madrid, Spain

Introduction

Coffee is one of the most popular and highly consumed food products in the world. According to the International Coffee Organization, during the 2012–2013 harvest, 145 million 60-kg bags were produced globally. The quality of coffee beverage is strongly related to the chemical composition of the roasted beans but is also dependent on the postharvest processing (Illy and Viani 2005). To produce coffee beans suitable for transport and roasting, there is a need to separate the seeds from the outer layers. Worldwide, coffee cherries are processed by either "dry" or "wet" methods to separate the beans from the pulp. In Colombia, Central America and Hawaii, the wet method is preferred for Arabica coffee (Mussatto et al. 2011). In this method, the coffee cherries are first depulped to remove the skin (exocarp) and the pulp (outer mesocarp). After a relatively short fermentation period (24–48 h), a water wash is used to remove the mucilage layer. The beans are then sun-dried to 12 % moisture content. The main

Published online: 15 May 2014

goal of fermentation is to degrade the slimy mucilage adhering firmly to coffee beans (Illy and Viani 2005). This mucilage is mainly composed of simple sugars and a pectic substrate (Garcia et al. 1991), which are converted to alcohols and organic acids exothermically. The production of these metabolites leads to a decrease in pH (Avallone et al. 2001) and a textural change is observed, after which washing can be used to remove this mucilage. Masoud and Jespersen (2006) and Peñuela-Martínez et al. (2010) suggest temperature and pH as the main control variables, which can be used to predict the end of the fermentation process. Several authors indicate that fermentation must be controlled to limit poor beverage quality (Bede-Wegner et al. 1997; Lopez et al. 1989; Murthy and Naidu 2011; Woelore 1993). However, in reality, fermentation is the least controlled step of the process, causing production plants to operate far from optimal conditions in terms of both operation costs (i.e. high energy and water consumptions) and final product quality (Barreiro et al. 2010). Research efforts are being exerted to develop novel, fast, non-destructive and accurate sensing techniques suitable for on-line process optimisation to provide information that is highly correlated to quality properties (Esteban-Diez et al. 2004).

Rapid advances in sensors and wireless communications have the potential to assist in managing the generation of large amounts of data by monitoring systems. Wireless sensor networks (WSNs) are a very promising technology in the field of product supervision and logistics, offering lower installation costs than wired devices and providing new opportunities for distributed-intelligence architectures (Maxwell and Williamson 2002; Wang et al. 2006). Among wireless technologies, radio-frequency identifiers (RFIDs), which are tags that include identification information, have been improved by incorporating a variety of sensors (e.g. temperature) to act as multi-distributed miniaturised loggers (Abad et al. 2007; Vergara et al. 2007). As an example of thermal monitoring, wireless intelligent sensors have been used inside refrigerated vehicles during international transport (Jiménez-Ariza et al. 2013; Lang et al. 2011), demonstrating that they can be used for the prediction of the emergence of warm spots (Jedermann et al. 2013). Only a few studies, such as those carried out by Avallone et al. (2001), Jackels and Jackels (2005) and Peñuela-Martínez et al. (2010), are related to the control and supervision of coffee fermentation. The literature on automatic systems for controlling fermentation based on wireless sensors is mostly focused on wine. Among them, Ranasinghe et al. (2013) propose measuring the temperature gradient across a fermentation tank with a sensor array constructed to accommodate seven wireless resistance temperature detectors capable of real-time monitoring of fermentation vats, while Di Gennaro et al. and Sainz et al. (Di Gennaro et al. 2013; Sainz et al. 2013) focus on wireless sensor communication issues.

The use of low-cost, wireless and autonomous sensors allows the installation of intensive and real-time data acquisition networks, which make feasible reconstruction of the temporal and spatial distribution of such variables as temperature from point measurements (Garcia et al. 2007). Models can be developed to explain and predict temperature changes, but plants are plagued by ever-present disturbances inducing dynamics that alter the validity of the models and promote both parametric and structural uncertainty. Optimisation involves searching on high-dimensional and complex (non-convex) state spaces, especially for dynamic scenarios. In this way, the phase space (or phase graph) is the most adequate representation of the behaviour of a dynamical system. In principle, we should know the corresponding differential equation system, solve it for a given set of initial conditions and then plot the solution in the phase space representation. However, as proven by Packard et al. (1980), Takens (1981), Eckmann and Ruelle (1985) and other authors, a topological approximation of the phase space of a dynamical system can be obtained from a time series corresponding to one of its solutions. That is, we can approximately reconstruct the phase space of an unknown dynamical system through a time series obtained by measuring one of its physical variables over time.

The objective of this work is to develop a new data analysis methodology based on the reconstruction of the spatial distribution of temperature and the implementation of phase space graphs to characterise the temperature gradients in a fermentation tank using multi-distributed, low-cost and autonomous wireless sensors.

Materials and Methods

Experimental Set-up

Coffee cherries (*Coffea arabica* var. Castillo, Borbón and Caturra) were handpicked at the mature stage in a plantation in Popayán (Cauca, Colombia). The external mesocarp was mechanically eliminated immediately after harvesting, and the depulped beans were left to natural fermentation. The fermentation began at 17:00 pm (sunset is at 17:44 pm in October), when outside temperature decreases, and ended at 9:50 am (sunrise is at 5:42 am) according to expert inspection. Thus, the fermentation was complete after 16.8 h.

The natural fermentation of coffee was carried out in a covered plastic tank in the shape of a frustum of a cone placed inside a warehouse. The tank, with a top diameter of 1.04 m and a height of 0.85 m, was filled with 276 kg of depulped coffee cherries to a tank fill level of 0.44 m (Fig. 1). This set-up is among those found in the region of Cauca, where heterogeneous tank designs are used depending on the characteristics of each coffee farm.

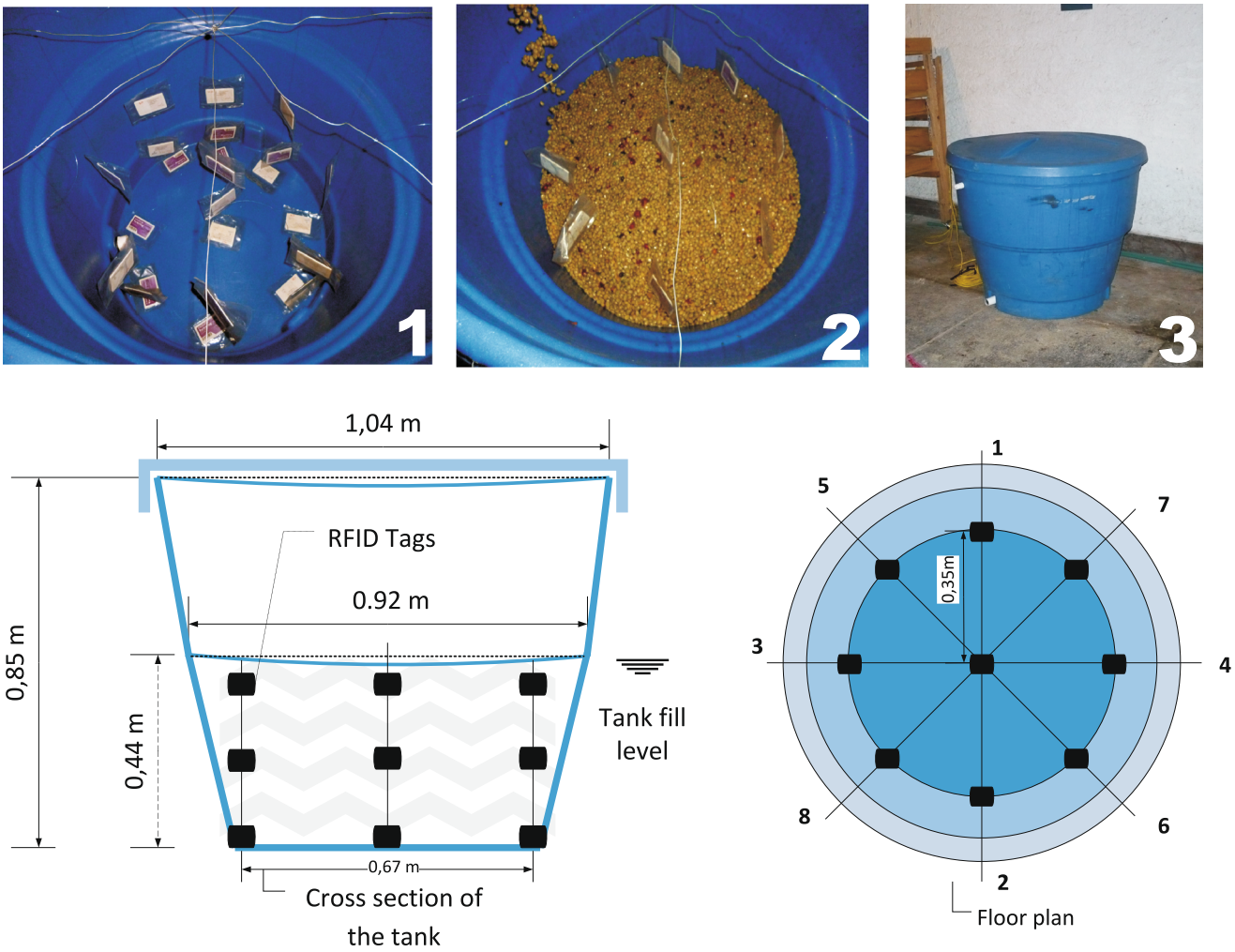

Fig. 1 Images of the experiment set-up (*top*): *1* sensor placement, *2* filling the tank and *3* fermentation. Scheme of the sensor distribution in the tank (*bottom*)

The multi-distributed sensor network consisted of 27 TurboTag® RFID tag temperature loggers (only 23 correctly collected the data). Each tag was protected by a resistant plastic material to guarantee impermeability and thereby prevent electrical short-circuiting from immersion in the fermenting mass. To remove the insulating effect of the air within the protective bag, it was removed using a vacuum. The accuracy of the temperature RFID tags is (from −30 °C to +40 °C)±0.5 °C. All communications with the T-700 series tags are carried out using a DR-1 RFID reader (13.56-MHz RFID interface), a small desktop USB device for use with a PC running Session Manager Software. Due to the 702 data points available as internal memory, a high temporal resolution of 2 min/data was used. The total number of acquired data points was 504 per sensor.

The sensors were equi-spatially distributed along eight radii (Fig. 1) and three horizontal planes parallel to the floor (ground, middle and surface levels). Eight sensors were placed at 0.33 m on each plane, and one sensor was placed at the centre (nine tags/plane in total). Due to battery failure and/or configuration mistakes, two perimeter tags on the middle plane (at radii 3 and 6 in Fig. 1) and two tags on the surface plane (at radii 1 and 2) did not correctly record the data. An additional tag was placed to register the ambient temperature.

Data Analysis

To facilitate the handling of data from the 23 RFID tags, a hierarchical clustering based on temporal series was performed to define groups of sensors. The matrix of Euclidean distances between each pair of individuals was calculated, grouping the closest individuals and hierarchically merging groups (or individuals) whose combination gave the smallest average linkage distance (that is, the average distance between all pairs of objects in any two clusters). A devoted Matlab® code was developed to generate groups of sensors based on the cluster tree features.

To analyse the recorded data, two different and complementary procedures were implemented.

First, polar interpolation using a dedicated Matlab® code was used to create 2D spatial representations of the temperature profiles corresponding to the three horizontal planes defined in the tank. Prior knowledge of the location of each tag in the plane allowed the polar coordinates to be defined, i.e. the radius (0 or 33 cm) and angle (0 to 2π radians in 2π/8-radian steps) and to the generation of an interpolation mesh grid (increasing the resolution of the spatial mesh by one order of magnitude). The interpolation mesh grid is used under the Matlab® function INTERP2 to compute the interpolated temperature values at the points defined in the new mesh grid. In those polar coordinates at which the RFID tags did not record temperature data, the average of the temperatures of the previous and next polar coordinates was used for interpolation. The function INTERP2 returns the interpolated values of a function of two variables at specific query points using linear interpolation. The results always pass through the original sampling of the function. The input of the function must include the coordinates of the sample points, the temperature values at these points and the coordinates of the interpolation mesh grid. The Matlab® function CONTOURF produces 2D surface plots with isolines representing equal temperatures and areas between isolines using constant colours. In our case, 50 steps were represented between the minimum and maximum temperatures registered during the fermentation process.

Second, the reconstruction of the phase space from the time series was carried out as outlined below. It is well known that a continuous dynamical system can always be described by a system of N differential equations in canonical form:

$$\frac{dy_i}{dt} = f_i(y_1, y_2, \ldots, y_N, t),$$

with $i=1,2,\ldots,N$, where y_i is the i-th physical magnitude evolving in time t. The overall representation $(y_1,y_2,\ldots,y_N)$ of the corresponding N solutions $y_i(t)$ is the so-called phase space. Notice that the behaviour of the system is determined by the structure of the phase space. Following Eckmann and Ruelle (see sec. II-G in Eckmann and Ruelle 1985), the best way to reconstruct the phase space from a time series is by using *time delays* (rather than the numerical time derivatives proposed by Packard et al.). The technique is as follows: Let the experimental time series be $Y_1^{(k)}=y_1(t_k)$ with $k=1,2,\ldots,M$, corresponding to M periodic measures (i.e. measures with the fixed time step $\tau=t_{k+1}-t_k$) of the physical magnitude y_1. We can then reconstruct the complete phase space including the remaining magnitudes (y_1, $y_2,\ldots,y_N$) in the discrete form of the corresponding time series $(Y_1^{(k)},Y_2^{(k)},\ldots,Y_N^{(k)})$ by making $Y_i^{(k)} = Y_1^{(k+\Delta_i)}$ with $i=1,2,\ldots,N$ and $\Delta_1=0$, where each non-negative integer Δ_i defines a time delay $t_{d_i} = t_{k+\Delta_i}-t_k = \Delta_i\cdot\tau$. Note that the time delay does not depend on the measure number k because the time step τ is fixed. That is, in terms of graphical representations, the phase space is reconstructed from a time series by the representation of the time series versus itself delayed in time, where the appropriate value for the time delay t_{d_i} and the system dimension N are obtained by heuristics. In this work, 2D ($N=2$) phase space representations have been obtained by plotting the measured temperature $T(k)$ at each time $t(k)$ versus the temperature $T(k+\Delta)$ at time $t(k+\Delta)$, with optimum $\Delta=10$ set up by heuristics. In this case, the data acquisition interval (i.e. the fixed time step of the time series) is $\tau=2$ min; thus, the corresponding time delay is $t_d=\Delta\cdot\tau=20$ min. To obtain the optimum time delay, different values of Δ have been systematically tested to find the maximum area of the trajectory loops in phase space. The area of the trajectory loops corresponding to one sensor or one group of sensors has been computed using the Matlab® function CONVHULLN. This function allows a set of points to be selected from the trajectory loop in the phase space plot and returns the smallest convex envelope containing the set of points and the corresponding area. The function CONVHULLN is based on the Quickhull (Qhull) algorithm for convex hulls (Barber et al. 1996).

The software STATISTICA 6.1 (StatSoft, Inc.) and the statistical toolbox of Matlab® version 7.0 (R14) were used to compute the basic statistics, including the mean, standard deviation and confidence intervals and to conduct the analysis of variance.

Results and Discussion

Temporal Information

Figure 2 presents the temperature dynamics inside the vat registered by the RFID tags throughout the fermentation process. Taking into account all data from the 23 tags, the average fermentation temperature was 21.2 °C, similar to that reported by Avallone et al. (2001) for a 20-h fermentation under similar conditions. The temperature inside the tank was higher than that outside the tank throughout the fermentation due to the activity of the mesophile microflora, as described in previous studies (Avallone et al. 2001). The lowest temperature registered was 19.0 °C, corresponding to a sensor located at the bottom of the tank, while the maximum temperature was registered at the centre of tank in the surface plane (23.6 °C). The average standard deviation (SD, $n=23$ sensors) was ±0.36 °C, value above the accuracy of ±0.19 °C estimated by Jedermann et al. (2009) for RFID tags, while the average spatial SD (calculated for sensors at different locations for the same instant, $n=504$ time data) was more than three times that value (±1.21 °C). Figure 2 also shows the average instant temperature throughout the fermentation, which is significantly ($p<0.05$) correlated with the ambient temperature, with a coefficient of correlation $r_{Pearson}=0.22$, according to a

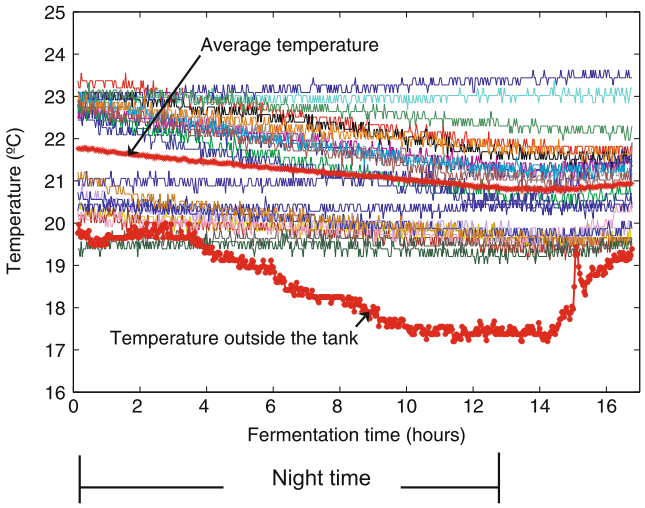

Fig. 2 Temperature dynamics inside the vat during the fermentation step (16.8 h) for 23 RFID tags (*thin lines*). The *thick line* with *red squares* represents the temperature registered outside the tank. The *thick red line* shows the average instant temperature (n=23 sensors) over the course of the fermentation process

fermentation process that occurs spontaneously under ambient temperature conditions.

In the clustering procedure, five groups were identified, labelled from A to E (Table 1). Group A, consisting of three RFID tags, corresponds to the hottest locations inside the tank (the centre of the surface and middle planes). Group B, corresponding to ten RFID tags, refers to the periphery of the surface and middle planes. Group C only includes one sensor, which is located in the middle plane near the average fermentation temperature. Group D, with seven RFID tags, is located at the floor of the tank. Finally, Group E, with two sensors, is located at the coldest location on the floor plane. One-way analysis of variance (ANOVA) (Fig. 3) showed that the five groups selected were significantly different (F=72.16, p<0.05), confirming the existence of five areas of different temperature behaviour in the tank during the fermentation process.

Spatial Information

Two-way ANOVA was carried out to analyse the effect of two factors, height and radial distance, with no significant interaction. The analysis showed that height had a relevant effect (F=41.4, p<0.05) on fermentation temperature, with the temperature decreasing from the top of the vat to the floor (Fig. 4). The radial distribution of sensors (centre and peripheral) was also significant (F=17.9, p<0.05), with the temperature being highest at the centre of the vat (Fig. 4). The tags located at the peripheral locations were more strongly correlated with the ambient temperature than the central area ($r_{Pearson}$=0.2±0.03 and 0.1±0.07, respectively).

Table 1 The 23 RFID tags clustered by group from A to E, their placement in the tank at different heights or levels (M: middle, S: surface, F: floor) and radii (C: centre, P: perimeter)

Group	A			B								C	D					E		
Tag ID	5	12	20	1	2	3	4	9	10	11	19	22	24	16	6	7	13	14	17	18	21	8	23
Level	M	S	S	S	S	S	M	S	M	S	M	M	M	M	F	F	F	F	F	F	F	F	F
Radius position	C	C	P	P	P	P	P	P	P	P	P	P	P	P	P	P	P	P	P	C	P	P	P
r	*0.16*	0.00	0.01	*0.26*	*0.14*	*0.18*	*0.21*	*0.09*	*0.18*	*0.21*	*0.23*	*0.12*	*0.21*	*0.36*	*0.10*	*0.17*	*0.55*	*0.19*	*0.24*	*0.15*	*0.17*	−0.04	*0.26*

The Pearson's correlation coefficient *r* for each tag located inside the tank with respect to the tag located outside is also shown (italic indicates a significant correlation)

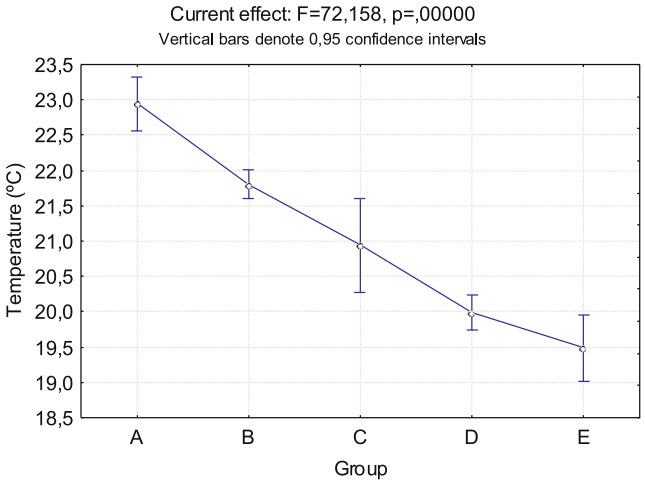

Fig. 3 Least-squares mean graph of the result of one-way ANOVA showing the effect of the factor "group of sensors" (from A to E) on the variable "temperature"

The existence of these temperature gradients is corroborated by Fig. 5, which shows the spatial distribution of temperatures in each plane of the tank at the beginning, middle and end of the fermentation process. At time $t=0$, the beans were heated in the mechanical removal of pulp and transferred to the fermentation vat. In this step, the temperature is highest and most homogeneous. However, the bottom of the vat presents a lower temperature than the other two planes due to the heat conduction through the concrete floor of the warehouse, even at $t=0$. Figure 5 shows that during the fermentation process, the surface and middle planes maintain a similar temperature profile, with the main vertical temperature gradient occurring from the middle plane to the floor plane. Between these two planes, the average temperature difference is 2 °C for a 15-cm height, with a maximum instant variation of 3.8 °C for sensors with equal polar coordinates (temperature gradient of 0.25 °C/cm). Such variation is comparable to that found in other fermentation processes (red wine), where automated control is recommended instead of time control based on the vertical temperature gradients. Ranasinghe et al. (2013) limits the maximum vertical allowed variation to 5 °C.

Figure 5 also shows that for every plane and every fermentation time, there is a radial temperature gradient corresponding to a radial heat transfer from the pseudo-cylindrical vat to the surrounding air. The maximum instant radial temperature gradient has been quantified as 0.1 °C/cm from the centre to the perimeter of the tank (3.3 °C in 33 cm). Figure 5 also shows that, once the fermentation process begins ($t=8$, $t=16$), the images corresponding to surface plane and middle plane are defined with a progressively higher number of contour lines than those for the floor plane, indicating higher gradients for the former than the latter.

On the other hand, Fig. 6 (top) shows the phase graph of the temperature series throughout the fermentation ($\Delta=10$, $t_d=10(\text{step})\cdot 2(\text{min/step})=20\,\text{min}$) for the five clusters of sensors identified (A to E). The sensors belonging to the same group appear in the same colour and in the same region of the phase graph. The areas of the polygons that include all of the data points of each individual sensor on the phase graph quantify the variability of the temperature for each location. Group A, with an average temperature of 22.9 °C, refers to the hottest points of the tank. These sensors also characterise a tank area with one of the most stable temperatures, as indicated by the small average area in the phase space (0.39 °C^2, $\Delta=10$; Fig. 6 bottom). Group E, with an average temperature of 19.5 °C, is located on the base of the phase graph (Fig. 6 top) with the smallest average area (0.25 °C^2, $\Delta=1$; Fig. 6

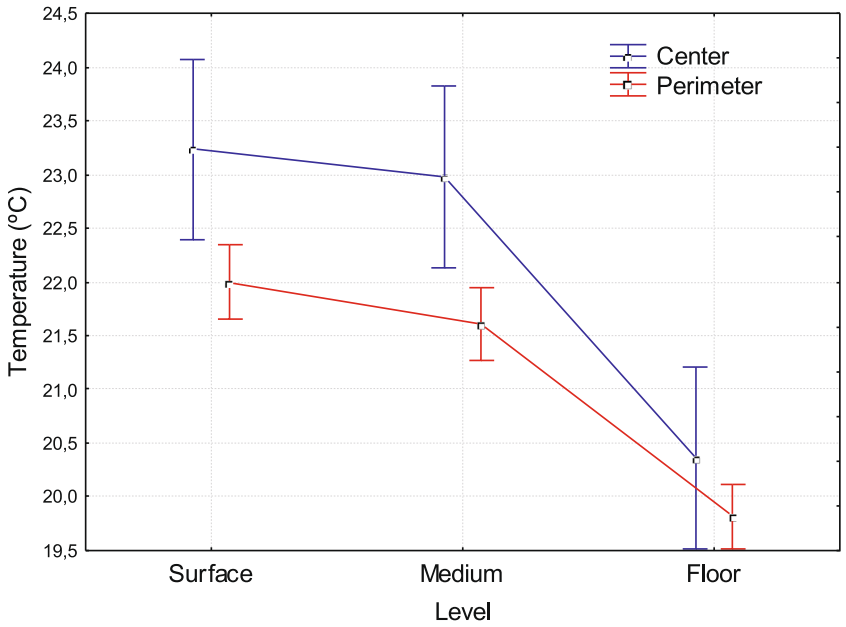

Fig. 4 Least-squares mean graph of the result of two-way ANOVA showing the effect of the factors "level" or placement of sensors in the tank at different heights (surface, middle or floor) and radii (centre or perimeter) on the variable "temperature". *Vertical bars* denote 0.95 confidence intervals

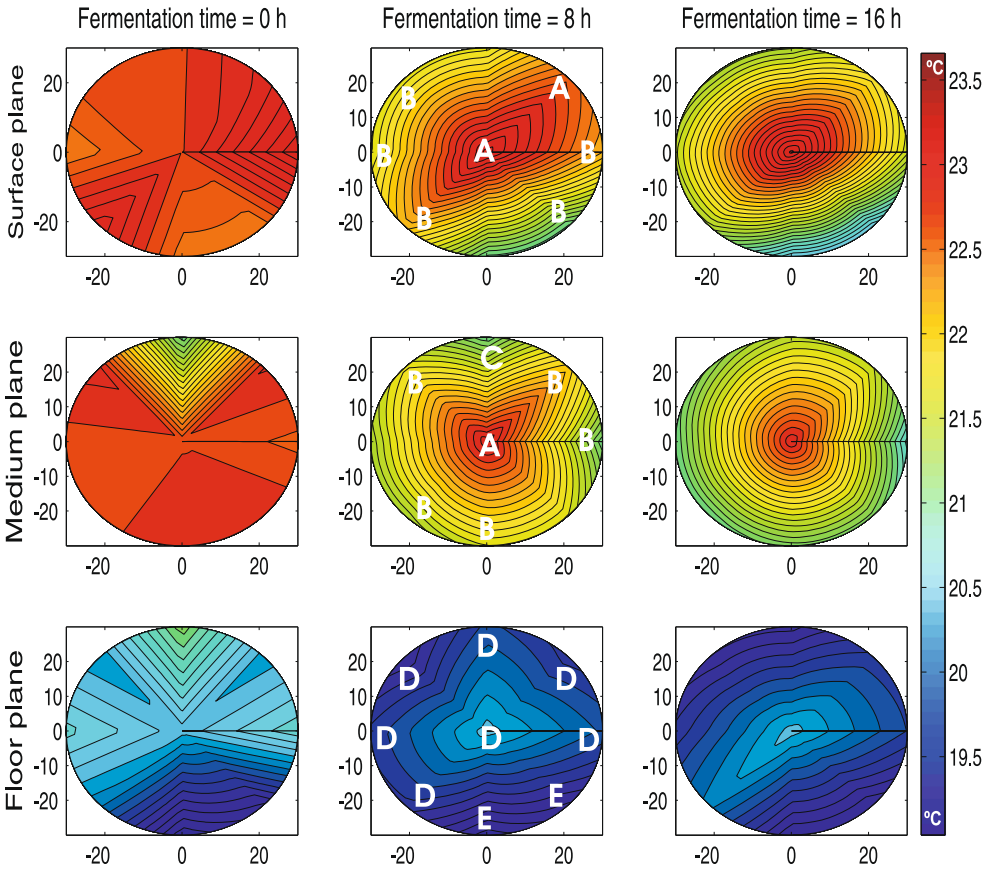

Fig. 5 2D surface plot of the temperatures interpolated along the radius of the tank (0–33 cm) for the three planes or height levels defined in the vat (surface, middle and floor). In this representation, three instants of time have been selected: the beginning (time 0 h), middle (time 8 h) and end (time 16 h) of the fermentation process. The location of the sensors on each plane according to the group (from A to E) to which they belong is also shown

bottom). Thus, it corresponds to the coldest and more stable points inside the vat. Group B, which includes the peripheral RFID tags located in the surface and middle planes, is the zone subjected to the highest temperature gradients, as indicated by its average area, which is the largest in the phase space (1.1 $°C^2$, $\Delta=10$; Fig. 6 bottom).

Therefore, the temperature series reconstructed as a 2D phase space in Fig. 6 (top) illustrates different patterns or attractors that allow a confined representation of several spatial behaviours throughout the fermentation process. Such attractors correspond to identified regions in the vat and are characterised by their shape and location in the phase graph. Pattern recognition based on phase graphs was also used in other research areas to identify different behaviours in time series (Huang et al. 2009; Jiménez-Ariza et al. 2013).

The phase graph of temperatures shows that inside the vat, Group A can be identified as one of the most stable areas of the tank in terms of temperature but is constantly subjected to high temperatures. Considering that coffee fermentation is carried out by aerobic, anaerobic, lactic, yeast and pectolytic microflora (Avallone et al. 2001; Masoud and Jespersen 2006) in an exothermic reaction, the rate of reaction is higher in this area than in the other areas, posing the risk of developing over-fermented beans in the time required for fermentation to be established in the rest of the tank. This may be related to the occurrence of defective sour and foul-smelling beans in a given coffee sample (Mancha Agresti et al. 2008). On the other hand, Group E corresponds to the coldest points inside the vat. It is interesting to note that the average temperature of Group E, 19.5 °C, is at the lower limit of the optimal range for the growth of mesophile bacteria (20–40 °C), including lactic acid bacteria, which are primarily responsible for the decrease of the pH of the medium. In agreement with Masoud et al. (Avallone et al. 2001; Masoud and Jespersen 2006), the optimal polygalacturonase enzyme secretion by yeasts is found at pH 6 and 30 °C, with variations between species and even between strains of the same species. Lower temperatures result in lower fermentation rates and lower enzymatic secretion, which could lead to a higher risk of incomplete mucilage breakdown and thus uncontrolled secondary fermentations during drying and storage (Woelore 1993).

Fermentation in the presence of the solid portions will not occur uniformly. The yeast and other microorganisms will have different levels of nutrients, and the temperature dissipation through the mass will occur at differing rates (Ranasinghe et al. 2013), leading to a heterogeneous temperature distribution throughout the process. This could result in the selection of different microbial groups according to temperature and thus the heterogeneity of fermented grain aromatic

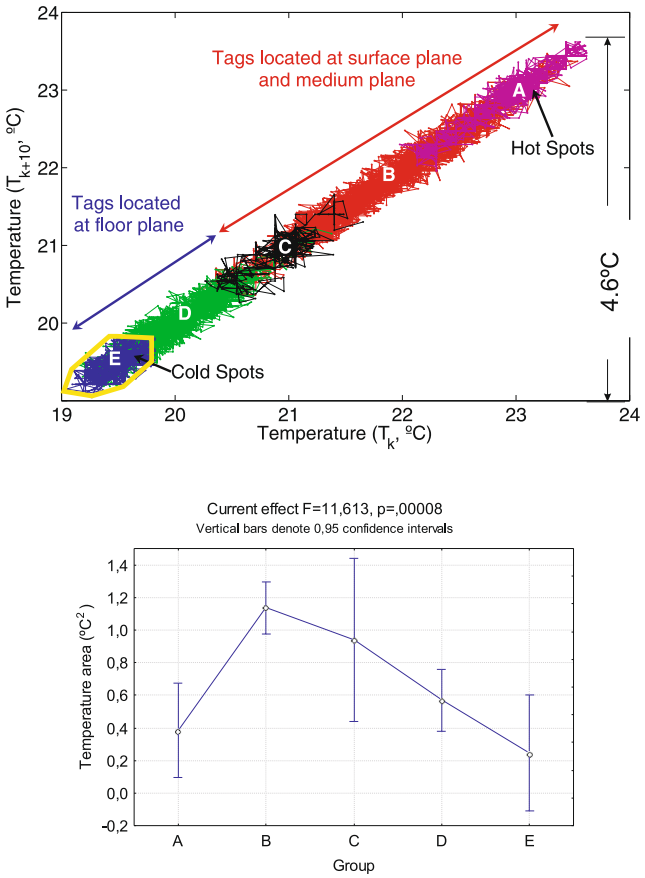

Fig. 6 Phase graph for temperature with $\Delta=10$ (t_d=10(step)·2(min/step)=20min) for RFID tag sensors (*top*): sensor groups A (*magenta*), B (*red*), C (*black*), D (*green*) and E (*dark blue*). The *yellow convex line* enveloping the area that contains the attractor corresponding to temperature data points of group E is indicated as an example of the graphic method used to compute the area of one attractor. Least-squares mean graph presenting the result of one-way ANOVA showing the effect of the factor "group of sensors" (from A to E) on the variable "temperature area" corresponding to the areas computed on the phase graph, shown in the *upper part* of this figure, for each sensor (*bottom*)

compounds, influencing the sensory characteristics of the coffee beverage.

Conclusions

This work applies spatial interpolation and phase space graphs as novel methodologies to demonstrate that significant temperature gradients occur within coffee fermenting tanks. The use of these two complementary methodologies allows a variety of consistent behaviours during fermentation to be identified and quantitatively characterised. To the best of the authors' knowledge, phase graphs have never been applied thus far to study the temperature in fermenters.

Spatial interpolation shows that the radial gradient is highest in the surface and middle planes and lowest in the floor plane. The maximum temperature variation has been bounded by RFID tags as 4.6 °C. The maximum instant radial temperature gradient has been quantified as 0.1 °C/cm from the centre to the perimeter of the tank. On the other hand, the vertical temperature gradient between the middle and floor planes reaches a maximum instantaneous value of 0.25 °C/cm for sensors with equal polar coordinates.

Phase graphs of the temperatures allow the recognition of patterns in a confined representation regardless of the size of the time series. In this way, hot and cold spots can be quickly identified. The area of the attractors computed within the temperature phase graphs is proposed as an indicator of the temperature variability. The average area for peripheral tags (1.1 °C^2) located at surface and middle planes was 4.4 times higher than those computed for the cold spot (0.25 °C^2) located at the floor plane, identifying the zone of the vat subjected to the highest temperature variations.

The temperature gradients found are the results of two combined effects: (1) heat dissipation from the non-insulated tank by convection towards the outside environment, mainly in the radial direction, and by conduction to the concrete floor of the warehouse and (2) the different kinetics of the exothermic reactions depending on the temperature and nutrient distributions in the fermenting mass. The lack of control favours the development of sensory defects in the final product because they may lead to local over-fermentations together with incomplete fermentations at other locations.

In this study, spatial interpolation and phase graphs have been applied to identify five differential temperature behaviours among 23 locations. This approach may be used to optimise the size of a sensor network while maintaining information relevancy. Such locations could become critical control points in the fermenter. Further work is being carried out with other coffee fermentations to validate these results.

These methodologies can be used for automated control of coffee fermentation, as temperature homogeneity is critical. The current availability of low-cost sensors (RFID tags cost approximately US$25) that are easy to install and do not interfere with the process facilitates the multi-distributed supervision of the temperature inside a tank. This work proposes the use of phase space graphs and spatial interpolation as a part of a decision support tool for monitoring the fermentation process and characterising fermenting tanks (locations of hot and cold spots). It is important to note that this procedure has potential applicability on any agro-food processes in which temperature is the control variable, such as wine fermentation, retort sterilisation or drying processes.

Acknowledgments This study was funded by the Spanish Government through the SMART-QC project (GL2008-05267-C03-03), UPM project CAFECOL (AL11-PID-30) and FRUTURA (109RT0383) International Net of CYTED. We also wish to thank the Technical University of Madrid and the International Campus of Excellence CEI Moncloa/UPM-UCM for their support.

References

Abad, E., Zampolli, S., Marco, S., Scorzoni, A., Mazzolai, B., Juarros, A., et al. (2007). Flexible tag microlab development: gas sensors integration in RFID flexible tags for food logistic. *Sensors and Actuators B-Chemical, 127*, 2–7. doi:10.1016/j.snb.2007.07.007.

Avallone, S., Guyot, B., Brillouet, J. M., Olguin, E., & Guiraud, J. P. (2001). Microbiological and biochemical study of coffee fermentation. *Current Microbiology, 42*, 252–256. doi:10.1007/s002840010213.

Barber, C. B., Dobkin, D. P., & Huhdanpaa, H. (1996). The Quickhull algorithm for convex hulls. *ACM Transactions on Mathematical Software, 22*, 469–483. doi:10.1145/235815.235821.

Barreiro, P., Correa, E.C., Arranz, F.J., Diezma, B., Ruiz-García, L., Villarroel, et al. (2010). Smart sensing applications in agriculture and food. In I. N. Y. Nova (Ed.), *Smart sensors: Technology, developments and applications*. Science Publishers.

Bede-Wegner, H., Bendig, I., W. H., R. W. (1997). Volatile compounds associated with the over-fermented flavour defect., 17th International Scientific Colloqium on Coffee, Association Scientifique Internationale du Café (ASIC), Nairobi. pp. 176–182.

Di Gennaro, S. F., Matese, A., Primicerio, J., Genesio, L., Sabatini, F., Di Blasi, S., et al. (2013). Wireless real-time monitoring of malolactic fermentation in wine barrels: the wireless sensor bung system. *Australian Journal of Grape and Wine Research, 19*, 20–24. doi:10.1111/ajgw.12006.

Eckmann, J. P., & Ruelle, D. (1985). Ergodic-theory of chaos and strange attractors. *Reviews of Modern Physics, 57*, 617–656. doi:10.1103/RevModPhys.57.617.

Esteban-Diez, I., Gonzalez-Saiz, J. M., & Pizarro, C. (2004). Prediction of sensory properties of espresso from roasted coffee samples by near-infrared spectroscopy. *Analytica Chimica Acta, 525*, 171–182. doi:10.1016/j.aca.2004.08.057.

Garcia, R., Arriola, D., Dearriola, M. C., Deporres, E., & Rolz, C. (1991). Characterization of coffee pectins. *Food Science and Technology-Lebensmittel-Wissenschaft & Technologie, 24*, 125–129.

Garcia, M. R., Vilas, C., Banga, J. R., & Alonso, A. A. (2007). Optimal field reconstruction of distributed process systems from partial measurements. *Industrial & Engineering Chemistry Research, 46*, 530–539. doi:10.1021/ie0604167.

Huang, B., Yan, G., Zan, P., & Li, Q. (2009). Study on gastric interdigestive pressure activity based on phase space reconstruction and FastICA algorithm. *Medical Engineering & Physics, 31*, 320–327. doi:10.1016/j.medengphy.2008.04.017.

Illy, A., & Viani, R. (2005). *Espresso coffee: the chemistry of quality*. U.K.: Academic Press Limited.

Jackels, S. C., & Jackels, C. F. (2005). Characterization of the coffee mucilage fermentation process using chemical indicators: a field study in Nicaragua. *Journal of Food Science, 70*, C321–C325.

Jedermann, R., Ruiz-Garcia, L., & Lang, W. (2009). Spatial temperature profiling by semi-passive RFID loggers for perishable food transportation. *Computers and Electronics in Agriculture, 65*, 145–154. doi:10.1016/j.compag.2008.08.006.

Jedermann, R., Geyer, M., Praeger, U., & Lang, W. (2013). Sea transport of bananas in containers—parameter identification for a temperature model. *Journal of Food Engineering, 115*, 330–338. doi:10.1016/j.jfoodeng.2012.10.039.

Jiménez-Ariza, T., Correa, E. C., Diezma, B., Silveira, A. C., Zócalo, A. C., Arranz, F. J., et al. (2013). The phase space as a new representation of the dynamical behaviour of temperature and enthalpy in a reefer monitored with a multidistributed sensors network. *Food and Bioprocess Technology*. doi:10.1007/s11947-013-1191-8. In press.

Lang, W., Jedermann, R., Mrugala, D., Jabbari, A., Krieg-Brueckner, B., & Schill, K. (2011). The "intelligent container"—a cognitive sensor network for transport management. *Ieee Sensors Journal, 11*, 688–698. doi:10.1109/jsen.2010.2060480.

Lopez, C.L., Bautista, E., Moreno, E., Dentan, E. (1989). Factors related to the formation of 'overfermented coffee beans' during the wet processing method and storage of coffee. In A. S. I. D. C. (ASIC) (Ed.), 13th, Paipa, Colombia. pp. 373–384.

Mancha Agresti, P. D. C., Franca, A. S., Oliveira, L. S., & Augusti, R. (2008). Discrimination between defective and non-defective Brazilian coffee beans by their volatile profile. *Food Chemistry, 106*, 787–796. doi:10.1016/j.foodchem.2007.06.019.

Masoud, W., & Jespersen, L. (2006). Pectin degrading enzymes in yeasts involved in fermentation of Coffea arabica in East Africa. *International Journal of Food Microbiology, 110*, 291–296. doi:10.1016/j.ijfoodmicro.2006.04.030.

Maxwell, D., & Williamson, R. (2002). Wireless temperature monitoring in remote systems. *Sensors, 19*, 26–30.

Murthy, P. S., & Naidu, M. M. (2011). Improvement of Robusta coffee fermentation with microbial enzymes. *European Journal of Applied Sciences, 3*, 130–139.

Mussatto, S. I., Machado, E. M. S., Martins, S., & Teixeira, J. A. (2011). Production, composition, and application of coffee and its industrial residues. *Food and Bioprocess Technology, 4*, 661–672. doi:10.1007/s11947-011-0565-z.

Packard, N. H., Crutchfield, J. P., Farmer, J. D., & Shaw, R. S. (1980). Geometry from a time-series. *Physical Review Letters, 45*, 712–716. doi:10.1103/PhysRevLett.45.712.

Peñuela-Martínez, A. E., Oliveros- Tascón, C. E., & Sanz-Uribe, J. R. (2010). Remoción del mucílago de café a través de fermentación natural. *Cenicafé, 61*, 159–173.

Ranasinghe, D.C., Falkner, N.J.G., Chao, P., Hao, W. (2013). Wireless sensing platform for remote monitoring and control of wine fermentation. In M. Palaniswami, et al. (Eds.), 2013 Ieee Eighth International Conference on Intelligent Sensors, Sensor Networks and Information Processing. pp. 503–508.

Sainz, B., Antolin, J., Lopez-Coronado, M., & de Castro, C. (2013). A novel low-cost sensor prototype for monitoring temperature during wine fermentation in tanks. *Sensors, 13*, 2848–2861. doi:10.3390/s130302848.

Takens, F. (1981). Detecting strange attractors in turbulence. Dynamical systems and turbulence. *Lecture Notes in Mathematics., 898*, 366–381. doi:10.1007/BFb0091924.

Vergara, A., Llobet, E., Ramirez, J. L., Ivanov, P., Fonseca, L., Zampolli, S., et al. (2007). An RFID reader with onboard sensing capability for monitoring fruit quality. *Sensors and Actuators B-Chemical, 127*, 143–149. doi:10.1016/j.snb.2007.07.107.

Wang, N., Zhang, N. Q., & Wang, M. H. (2006). Wireless sensors in agriculture and food industry—recent development and future perspective. *Computers and Electronics in Agriculture, 50*, 1–14. doi:10.1016/j.compag.2005.09.003.

Woelore, W.M. (1993). Optimum fermentation protocols for Arabica coffee under Ethiopian conditions. In A. s. i. d. c. (ASIC) (Ed.), 15th International Scientific Colloqium on Coffee, Montpellier. pp. 727–733.